ELSEVIER

International Journal of Solids and Structures 41 (2004) 569–584

INTERNATIONAL JOURNAL OF SOLIDS and STRUCTURES

www.elsevier.com/locate/ijsolstr

The response of a glass fibers reinforced epoxy composite to an impact loading

E. Zaretsky, G. deBotton *, M. Perl

Department of Mechanical Engineering, The Pearlstone Center for Aeronautical Engineering, Ben-Gurion University of the Negev, Beer–Sheva 84105, Israel

Received 24 June 2002; received in revised form 1 January 2003

Abstract

The dynamic response of a woven glass fibers reinforced epoxy composite to a planar impact loading is investigated. The composite samples were struck perpendicular to the fibers plane by aluminum 6061-T6 impactors at velocities ranging from 60 to 280 m/s. The free surface velocity of the samples was monitored by VISAR. To highlight the contribution of the resin's properties versus the role of the composite's microstructure analogous measurements were carried out on free-of-fibers homogeneous epoxy resin samples. Low-velocity impacts were performed to examine the response of undamaged specimens. Damage processes during the tensile and the compressive stages were activated by application of intermediate and high-velocity impacts.

At low-impact velocities the behavior of the composite is primarily dictated by the viscous behavior of the epoxy resin. The role of the microstructure becomes more noticeable at higher impact velocities. Oscillations of the free surface velocity profiles, originating from the reflection and refraction of the waves at the interior interfaces of the composite are observed. Owing to the composite's microstructure the acceleration duration of the free surface was notably longer than the corresponding duration measured for the homogeneous epoxy samples. It was further found that the compression wave speed increases with the pressure. In contrast with the epoxy samples, in undamaged composite samples the speeds of the compression and release waves are almost identical. Reduction in the release wave speed takes place only after some compression related damage accumulates in the composite. The spall strength of the composite is lower than the one measured for the epoxy but the post spall damage mechanism is somewhat slower.

1. Introduction

In recent years attention was given to the study of the transient behavior of composite materials under dynamic loading conditions. The characterization of the composite's behavior is complicated because of the numerous parameters that effect its response. Among these parameters are of course those that dominate the behaviors of the reinforcement and the filler, including strain-rate effects and various failure mechanisms. Important parameters, which provide the ability to control the elastic symmetries of composites

* Corresponding author. Address: CALTECH, Mechanical Engineering and Applied Mechanics, Mail Code 104-44, Pasedena 91125, USA. Tel.: +1-626-395-3002; fax: +1-626-568-2719.

E-mail address: debotton@caltech.edu (G. deBotton).

0020-7683/$ - see front matter © 2003 Elsevier Ltd. All rights reserved.
doi:10.1016/j.ijsolstr.2003.09.026

according to their designated usage, are the reinforcement volume fraction, geometry, and the spatial arrangement within the filler. The contrast between the impedance of the constituents results in reflections and refractions of the waves in the medium, and the properties of the interface have an important influence on the composite's behavior too. A review of some published works, summarizing common testing techniques and issues concerning the behavior of composites, can be found in Barre et al. (1996). In the present work the results of a series of plane impact experiments involving a common glass fiber reinforced epoxy composite is presented and some of the above mentioned issues are discussed.

Within the framework of the present study, where relatively low impact stresses were applied, the reinforcing glass fibers can be treated as linear-elastic. However, the behavior of the epoxy matrix needs to be characterized. A comprehensive discussion regarding the propagation of stress waves in polymers with nonlinear stress–strain relations and strain-rate dependence was carried out by Barker and Hollenbach (1970). It was demonstrated that in agreement with corresponding theoretical findings (Schuler, 1970) velocity profiles of materials with strain-rate dependent constitutive law are characterized by rapid initial rise time and gradual convergence to the peak velocity afterwards. Munson and May (1972) examined the behavior of Epon 828 based epoxy and its dependence on the chemical composition and the molecular structure. Based on a series of experiments, they provided estimates for the Rankine–Hugoniots of three epoxy compositions with different hardeners. It was further found that at high impact velocities the relevancy of the specific hardener used is diminished. El-Habak (1991) studied the behavior of glass fiber reinforced composites by application of a split Hopkinson pressure bar (SHPB) technique. It was found that the overall response of the composite is almost independent of the treatment applied to the fibers but sensitive to the resin type and the fibers volume fractions.

Straining-rate effects on the behavior of epoxy samples and glass fibers reinforced epoxy systems were experimentally studied by Tay et al. (1995). An Instron machine was used to characterize the behavior at low strain-rates and the SHPB method for higher strain-rate measurements. The behavior of the composite normal to the fibers plane was dominated by that of the epoxy filler. It was also found that the dependence of the response of both materials on the strain-rate is more pronounced at low strain-rates. An empirical constitutive law which accounts for the straining-rate effects was proposed as well. The viscoelastic behavior of a particulate composite induced from the behavior of the filler was studied by Munson et al. (1978). These investigators studied the transient behavior of Al_2O_3 reinforced epoxy composites under one-dimensional shock loading conditions. Numerical simulations in which a viscous Maxwell type model was assumed provided fair estimates for the corresponding experimental measurements. In this work, the transient behavior of the epoxy resin was examined by plane impact experiments with epoxy samples manufactured in a manner similar to the one followed for the composite samples.

The relevancy of the constituents' properties depends on the reinforcement spatial arrangement and volume fraction. Along the fiber direction the response is predominated by the behavior of the reinforcement while perpendicular to the fibers, or in particulate composites, the overall behavior is dictated by that of the filler. Lifshitz (1976) measured the variation in the uniaxial behavior of glass fibers reinforced epoxy composites as a function of the fibers orientation. The initial slopes of the stress–strain curves were found to be in agreement with quasi-static measurements and theoretical values based on homogenization theories for all measured orientations. The subsequent sections of the stress–strain curves as well as the tensile strength under dynamic loading, while in general higher than corresponding quasi-static values, strongly depend on the orientation of the fibers. Barker (1971) examined the strain rate dependency of the dynamic response of a laminated composite whose constituents' behavior is strain rate independent. An homogenized model for determining the Hugoniot of mechanical mixtures was proposed by Munson and Schuler (1971). Comparison of numerical estimates based on this model with corresponding experimental findings exhibited a favorable agreement. Holmes and Tsou (1972) determined the Hugoniot of aluminum fibers reinforced epoxy composites from measurements of shock wave and free surface velocities. Samples with various volume fractions of fibers were studied under plane impact conditions along the fibers. It was

found that expressions developed by Tsou and Chou (1969) for Hugoniot of composites in terms of the constituents behaviors and volume fractions provided good estimates for the measured data. The behavior of a glass fibers reinforced epoxy composites normal to the fiber direction was examined by Zhuk et al. (1994), free surface velocities and pressure variations during one dimensional impact experiments were measured, from which estimates for the Hugoniot of the composite were deduced. The relationship between the composite transient behavior normal to the fibers plane and the behavior of the epoxy filler are discussed in the course of the present work.

Refraction and reflections of waves propagating in a laminated medium were discussed by Postma (1955). It was demonstrated that laminated medium can be treated as an effective homogeneous medium only in the limit when the thickness of the layers is substantially smaller than the characteristic time of the stress pulse. Munson et al. (1978) obtained fair estimates for the behavior of particulate Al_2O_3 reinforced epoxy composites, where the particles size is small, by application of an homogenized model based on the self-consistent scheme. Lundergan and Drumheller (1971) examined the response of a steel-epoxy laminated composite to a planar impact both experimentally and analytically. Oscillations of the free surface velocity profile were detected and it was found that the peak amplitude of the stress decreased together with the width of the input pulse. Oved et al. (1978) identified strong oscillations of the stress pulse in a copper-PMMA laminated composite subjected to a one-dimensional impact conditions. The oscillations period was equal to twice the time it takes for the signal to travel across a pair of layers. The role of the interface and bonding quality between the phases was studied by Agbossou (1995). It was found that under dynamic loading conditions the off-axis response of a unidirectional fiber reinforced composite strongly depends on the interface quality. The structure of the composite considered in this work is characterized by two hierarchical levels. A fine sub-ply level of woven glass fibers fabrics embedded in an epoxy resin and a cruder laminated structure of 12 plies bonded with thin layers of epoxy adhesive. The refractions and reflections of the waves between the plies are clearly identified while traces of the heterogeneity at the fine level cannot be detected.

Spall strength of glass fibers reinforced epoxy composites were measured by Zaretsky et al. (1997). It was found that three possible deformation modes for the composite resulted in large variations of the spall strength. A nucleation and growth model together with a fracture model that were applied by Tokheim et al. (1989), provided good estimates for corresponding experimental measurements of spall strength in a Kevlar fibers reinforced epoxy composite. Delamination strength of glass fibers reinforced composites were measured by Dandekar et al. (1998) under plane normal and oblique impact conditions. A threshold shock induced compression stress beyond which delamination will occur due to refracted tensile waves was determined. The value of the threshold and delamination tensile stresses were found to depend strongly on the angle of the impact relative to the fiber's plane. Syam et al. (2000) examined the fracture mechanism in reinforced plastics. It was found that the damage zone consisted of matrix cracking, fractured fibers and debonding between the fibers and the matrix.

The objective of this work is to study the dynamic response of a woven glass fibers reinforced epoxy composite to impact loading normal to the fibers direction. The responses of samples made of both pure homogeneous and fiber-reinforced epoxy, were studied in a series of planar impact experiments. During these experiments the samples' free surface velocity was continuously monitored by VISAR (Barker and Hollenbach, 1972). A description of the experimental set up, the samples and the impacts parameters is given in Section 2. The measurements results, in terms of free surface velocity profiles, are presented and analyzed in Section 3. Finally, the main findings are summarized in Section 4.

2. Materials and experimental setup

Plane sheets of epoxy samples and laminated glass fiber reinforced epoxy 7781 composite samples (manufactured by "Orlite", Israel) were tested. The epoxy samples were prepared according to the

composite's manufacturer instructions. A mixture of 74% XB3485 resin and 26% 3486 hardener was prepared, heated to 70 °C for 2.5 h, then to 100 °C for 5 h, and finally cured to room temperature. To avoid the entrapment of air bubbles the samples were evacuated during the entire heating and curing cycle. The measured density of the epoxy was $\rho^{(e)} = 1120 \pm 3$ kg/m^3. From ultrasonic measurements it was found that the shear and the longitudinal sound velocities are

$$C_s^{(e)} = \sqrt{\mu^{(e)}/\rho^{(e)}} = 1150 \pm 30 \text{ m/s},$$

and

$$C_L^{(e)} = \sqrt{E'^{(e)}/\rho^{(e)}} = \sqrt{\left(K^{(e)} + \frac{4}{3}\mu^{(e)}\right)\Big/\rho^{(e)}} = 2700 \pm 20 \text{ m/s},$$

respectively. Throughout, E' denotes the constrained Young's modulus such that under a uni-dimensional straining condition the relation between the stress σ and the strain ε is $\sigma = E'\varepsilon$. These result in shear, constrained Young and bulk moduli for the epoxy $\mu^{(e)} = 1.48 \pm 0.04$ GPa, $E'^{(e)} = 8.16 \pm 0.01$ GPa and $K^{(e)} = 6.20 \pm 0.05$ GPa, respectively. The latter yields a bulk sound velocity for the epoxy

$$C_0^{(e)} = \sqrt{K^{(e)}/\rho^{(e)}} = 2350 \pm 30 \text{ m/s}.$$

According to the data sheet supplied by the manufacturer, the composite's density is $\rho^{(c)} = 1830$ kg/m^3. The composite samples were fabricated from 12 woven glass fibers reinforced epoxy plies. The thickness of each ply is 250 μm and is made out of two parallel 125 μm spaced layers of glass woven whose woofs and wefts are 30 μm bundles of about 50 glass fibers. The minimum distance between the bundles in a single woven layer varies from 10 to 50 μm. Approximately, the fibers volume fraction is $f^{(g)} = 0.45$. The overall thickness of the tested sheets varied between 3.09 and 3.16 mm. According to the spatial arrangement of the fibers the composite's elastic symmetry is an orthotropic one with identical behavior in the 0° and the 90° directions. Six constants are required to describe the constitutive relationship for materials having such a symmetry. According to the manufacturer's data sheet, the shear modulus in the fibers plane is $\mu_L^{(c)} = 4.0$ GPa, and the Young's modulus in the 0° and 90° directions is $E_L^{(c)} = 23.5$ GPa. From ultrasonic measurements the longitudinal and shear wave speeds normal to the fibers plane are $C_L^{(c)} = 2880 \pm 50$ m/s and $C_s^{(c)} = 1460 \pm 30$ m/s. The corresponding moduli are $E'^{(c)} = 15.2 \pm 0.4$ GPa and $\mu_T^{(c)} = 3.9 \pm 0.2$ GPa. Note that the shear moduli along and normal to the fibers plane are almost identical.

Planar impact experiments were performed with a 25 mm diameter, 3 m long gas gun and both composite and epoxy samples were studied. The impacts were produced by 6061-T6 aluminum alloy impactors of different thickness glued to hollow aluminum sabots which were accelerated to velocities in the range between 60 and 300 m/s. Electrical charged pins were used for measuring the impact velocity and for controlling the impactor–sample misalignment (tilt), which did not exceed 0.5 mrad. During the impact the velocity of the free surface of the samples was continuously monitored by VISAR. To enhance the intensity of the laser light reflected from the samples, a 10 μm aluminum foil was bonded to their free surface. The impact velocities and the thickness of the samples and the impactors for nine experiments are listed in Table 1. In all experiments the specimens and the impactors diameters are 24.7 mm. Since the epoxy occupies more than a half of the composite's volume it was decided to examine first the dynamic response of pure, free of fibers epoxy. The loading–unloading and spall behaviors of the epoxy were studied in three experiments. The composite samples were studied in the remaining six experiments. In all shots with the composite samples the impact direction was normal to the fibers plane.

Table 1
Impact velocities and samples' dimensions

Shot	Sample material	Impact velocity [m/s]	Impactor thickness [mm]	Sample thickness [mm]
AE	Epoxy	60[a] (5)	1.00	2.06 (0.02)
BE	Epoxy	244 (10)	1.00	2.43 (0.02)
CE	Epoxy	280 (10)	6.15	2.11 (0.02)
AC	Glass/epoxy	70 (5)	3.11	3.13 (0.01)
BC	Glass/epoxy	65 (5)	6.13	3.16 (0.01)
CC	Glass/epoxy	83 (5)	5.06	3.11 (0.01)
DC	Glass/epoxy	144 (10)	5.06	3.09 (0.01)
EC	Glass/epoxy	154 (10)	5.06	3.12 (0.01)
FC	Glass/epoxy	281 (10)	5.06	3.12 (0.01)

[a] Maximal errors associated with impact velocity and sample thickness measurements are given in the parentheses immediately after the measured value. The maximal error associated with the impactor thickness measurements does not exceed 0.002 mm.

3. Results

Free surface velocity profiles obtained after plane impact experiments with epoxy samples are shown in Fig. 1. The dots correspond to the experimental measurements. For convenience, the profiles are shifted one from the other by 0.5 μs along the time axis. The experimentally measured instant of the beginning of the velocity ramp was very close to that calculated on the basis of the ultrasonic measurements via the relation

$$T = \frac{\delta}{C_{\mathrm{L}}^{(\mathrm{e})}}, \tag{1}$$

where δ is the sample's thickness. It was decided to accept the time interval T from (1) as the starting point of the surface velocity ramp in all shots with the epoxy samples, although it is known that the shock wave

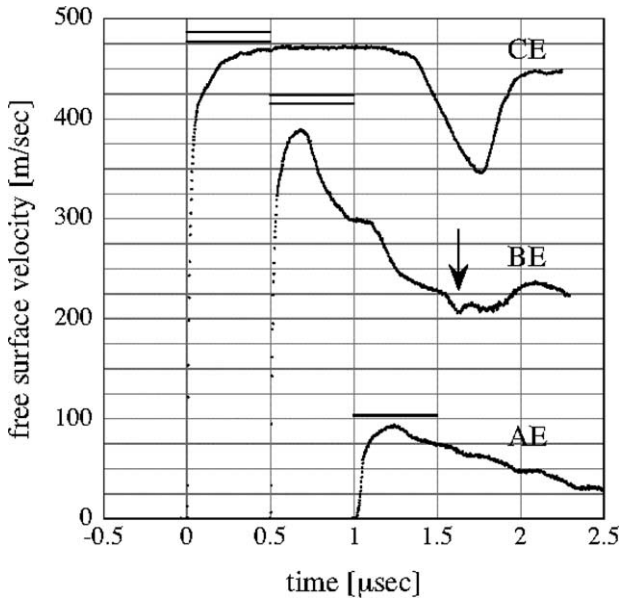

Fig. 1. Free surface velocity profiles measured for the epoxy samples.

velocity D increases with the increase of the impact strength. The thickness of the samples and the accuracy of flush mutual lapping of the epoxy sample body and the steel-copper pins were insufficient for accurate measurements of D. The three pairs of parallel solid lines in Fig. 1 show the expected response of the epoxy within an acoustic approximation based on the known impact velocity v_i and the values of the epoxy and the 6061 alloy moduli. The corresponding maximal free surface velocity of the sample is

$$w = \frac{2z^{(\mathrm{al})}}{z^{(\mathrm{al})} + z^{(\mathrm{target})}} v_i. \tag{2}$$

The value for the epoxy acoustic impedance $z = \rho^{(e)} C_L^{(e)}$ yields the bottom solid line for each shot, while the upper line was obtained with $z = \rho^{(e)} C_0^{(e)}$ assuming total relaxation of the shear stresses in the epoxy. The properties taken for the 6061 aluminum alloy are $\rho^{(\mathrm{al})} = 2703$ kg/m^3 and $C_L^{(\mathrm{al})} = 6380$ m/s. The fact that the maximum free surface velocities in shots AE and BE are lower than the estimates from (2) is due to the thin 1 mm impactors used in these shots. Thus, the head characteristic of the first unloading wave generated at the impactor's back surface has a propagation speed higher than the shock wave and overtakes it before its arrival to the sample's free surface. The arrival of several subsequent unloading waves are seen in the profiles obtained for shots AE and BE. In shot BE the meeting of two unloading waves, the first generated at the impactor's back surface and the second produced by the reflection of the initial shock from the sample's free surface, resulted in a spall of the epoxy sample. The instant, corresponding to the arrival of the spall signal to the sample's free surface is highlighted by the arrow in Fig. 1.

The steep initial rise of the three velocity profiles depends on the impact strength. This part of the velocity profiles may be analyzed within the framework of the simple wave approximation. Assuming that the free surface velocity w is twice the particle velocity u behind the compression wave, the stress and the strain, both related to the corresponding particle velocity, may be determined via the relations

$$\Delta\sigma = \rho_0 C \frac{\Delta w}{2}, \tag{3}$$

and

$$\Delta\varepsilon = \frac{\Delta w}{2C}, \tag{4}$$

respectively. Here $C = C(w)$ is the propagation speed of the stress signal, corresponding to the sample free surface velocity w. This is extracted from the arrival time T of the free surface velocity signal via the relation $C(w) = \delta/[T + \Delta t(w)]$. The corresponding compression curves obtained for the three shots with the epoxy samples are shown in Fig. 2a.

It is noted that the initial stress ramping follows the relation $\sigma = E'\varepsilon$. After the final impact pressure is achieved in shot CE the corresponding compression curve intersects the pressure curve $p(\varepsilon)$ which is obtained by integrating the equation

$$\Delta p = \rho_0 C_0^2 \Delta\varepsilon/(1 + s\varepsilon)^2. \tag{5}$$

The initial (small ε) slope of $p(\varepsilon)$ is equal to $K^{(e)} = \rho_0 C_0^2$ and the parameter s describes the dependence of the bulk modulus on the volumetric strain. According to Munson and May (1972) for different types of epoxies the approximation $s = 1.5$ is a reasonable one. Thus, the equality $\sigma = p$ at the final loading stage implies that the compressive path of the loading is terminated with a complete relaxation of the deviatoric stress component $S = \sigma - p$. The variations of the deviatoric stress component during the compression stage of all three shots are depicted in Fig. 2b.

The variations of $\dot{e}(t)$, the deviatoric component of the straining rate, during the compression stage were determined for the individual shots according to Eq. (4). We recall that under uni-dimensional straining conditions $e = \frac{2}{3}\varepsilon$. In Fig. 3 the variations of $\dot{e}(t)$ for shot CE are depicted. Also shown in the figure are the

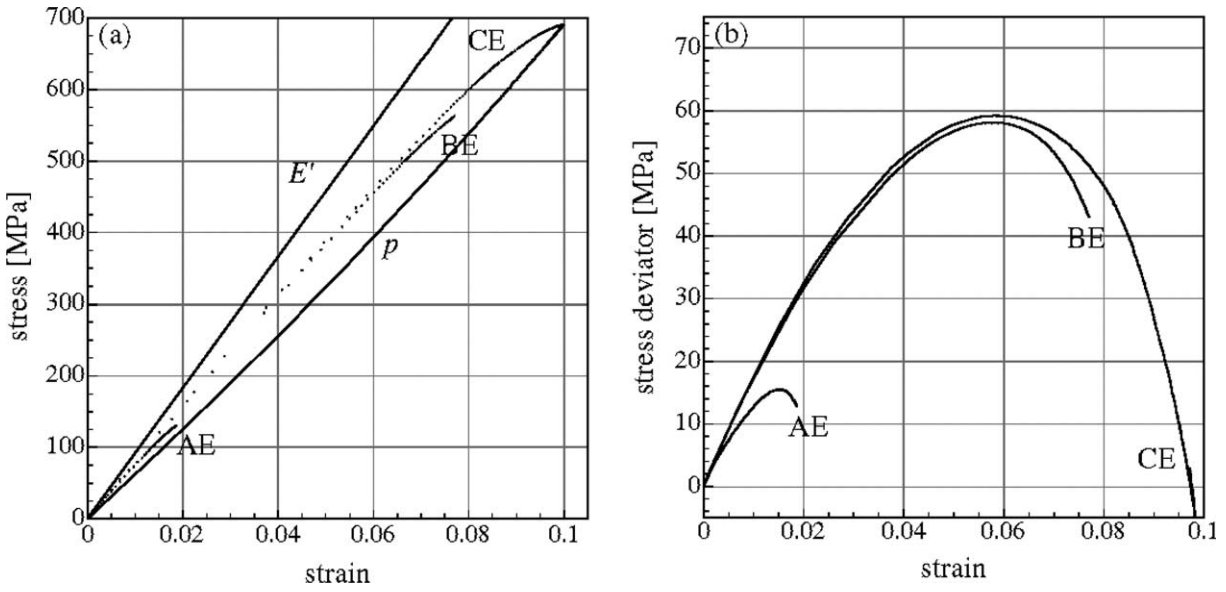

Fig. 2. Variations of the stress (a) and stress deviator (b) during the initial stages of the experiments with the epoxy samples.

variations of the deviatoric component of the stress rate $\dot{S}(t)$ normalized by $2\mu^{(e)}$. We note the agreement between these two curves at the instance when the front of the compression signal arrives at the free surface. After the initial rapid decrease of both curves $\dot{e}(t)$ slowly decreases to zero. The deviatoric component of the stress rate is fixed and negative, suggesting that $S(t)$ slowly decreases too. Thus, it follows that during the loading stage the viscoelastic behavior of the epoxy under shear may be approximated by the Maxwell model (a damper and a spring in a series). Following the notation of Kolsky (1963), this constitutive relation may be expressed in the form

$$\dot{e} = \frac{\dot{S}}{2\mu^{(e)}} + \frac{S}{2\eta^{(e)}}, \tag{6}$$

where $\eta^{(e)}$ is the dynamic viscosity. From the two curves shown in Fig. 3 together with the corresponding curve for S, the value of $\eta^{(e)}$ can be extracted by making use of Eq. (6). For the three shots with the epoxy samples it is found that $\eta^{(e)} \cong 110$ Pa s. According to the Maxwell model the relaxation time is $\tau^{(e)} = \eta^{(e)}/\mu^{(e)} = 75$ ns. In Fig. 3 the variations of $S(t)$ normalized by $2\eta^{(e)}$ are also shown together with the Maxwell estimate which is obtained by adding up the two curves for the terms on the right of Eq. (6). The approximate Maxwell type relationship between the deviatoric components of the stress and the strain implies that the studied epoxy may be interpret as a Standard-linear solid corresponding to a Maxwell element in parallel with an auxiliary elastic element. The elastic element corresponds to the behavior of the epoxy under dilatational loading.

The unloading part of the velocity profile BE (Fig. 1) is produced by a series of decremental pressure pulses arriving from the rear surface of the thin 1 mm aluminum impactor. On account of the isentropic character of the unloading process one can estimate the unloading isentrope of the epoxy for this shot. The peak epoxy stress in this shot was 560 MPa. This value is lower than the HEL of the 6061-T6 alloy. Accordingly, the unloading part of the shot may be analyzed while assuming that the response of the impactor is purely elastic. Note that the density of the epoxy when subjected to a pressure of 560 MPa is 1220 kg/m^3. A time-propagation distance diagram for this shot provides the isentropic velocities $C_s^{(e)}$ of the

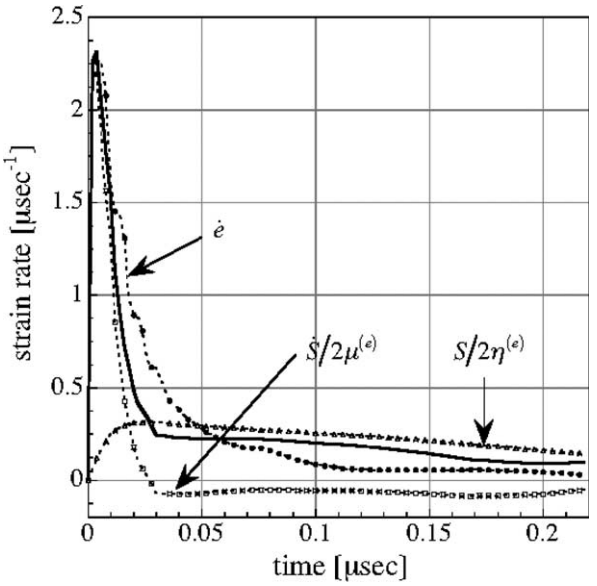

Fig. 3. Temporal variations of the strain-rate deviator (dashed curve with dark circles), the stress rate deviator normalized by the shear modulus (dashed curve with clear squares), the stress deviator normalized by the dynamic viscosity (dashed curve with clear triangles), and the corresponding Maxwell estimate (continuous curve) for shot CE.

subsequent unloading signals bringing the incremental stress levels from the impactor–sample interface to the sample's free surface. Applying the mass and momentum conservation laws to these subsequent unloading waves and accounting in that $C^2 = (\mathrm{d}p/\mathrm{d}\rho)$ along the isentrope yields the unloading isentrope for the epoxy up to a pressure of 560 MPa. The parameters of this unloading isentrope are listed in Table 2. The Rayleigh line for the loading together with the unloading isentrope are presented in the stress–particle velocity diagram of Fig. 4.

The velocity profile for shot BE allows to estimate the dynamic tensile strength (spall strength) $\sigma^{(e)}_{\mathrm{spall}}$ of the epoxy. Although the shape of the dynamic tension curve of the epoxy is unknown the value of $\sigma^{(e)}_{\mathrm{spall}}$ may be approximated from the pullback velocity $\Delta w = 181$ m/s measured from the velocity profile via the relation

$$\sigma_{\mathrm{spall}} = \tfrac{1}{2}\rho_0 C\,\Delta w, \tag{7}$$

where $\rho_0 C$ is an acoustic impedance (slope of the tension curve) whose value is between $\rho^{(e)}_0 C^{(e)}_{\mathrm{L}}$ and $\rho^{(e)}_0 C^{(e)}_0$. According to these two estimates for the acoustic impedance the corresponding approximations for the spall strength are, respectively $\sigma^{(e)}_{\mathrm{spall}} = 270$ MPa and $\sigma^{(e)}_{\mathrm{spall}} = 240$ MPa. The actual value of the epoxy spall

Table 2
Parameters of the release isentrope of the epoxy

Pressure [MPa][a]	Density [Kg/m^3]	Particle velocity [m/s]	Sound velocity [m/s]
0	1130 (5)	30 (5)	2700[b] (20)
210 (10)	1158 (5)	102 (3)	2780 (30)
370 (10)	1178 (5)	153 (3)	2870 (30)
560 (10)	1220 (5)	211 (3)	3050 (30)

[a] Approximate inaccuracies associated with these estimates are given in the parentheses immediately after the estimated value.
[b] From ultrasonic measurements.

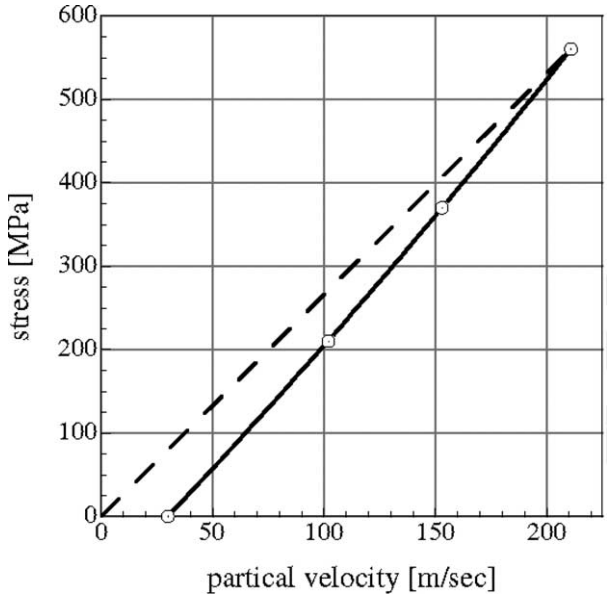

Fig. 4. Stress–particle velocity diagram for the Rayleigh line (dashed curve) and the unloading isentrope of the epoxy (continuous curve).

strength is probably at some intermediate value. The slope of the velocity profile before the appearance of the spall mark reflects a specific volume expansion rate $\dot{V} = \dot{w}/2\rho_0 C$ (see Eq. (4)). Following Utkin (1993), we deduce that since the section of the free surface velocity profile just after the arrow in Fig. 1 is horizontal, the damage rate of the epoxy $\dot{V}_{\mathrm{d}}^{(\mathrm{e})}$ is approximately four times the expansion rate. Therefore, during the spallation initial stage the damage rate is $\dot{V}_{\mathrm{d}}^{(\mathrm{e})} \approx 66\ \mathrm{m^3/kg\,s}$. Later on, the acceleration of the free surface indicate that the damage rate increases due to coalescence of previously produced voids up to the final separation of the spalled segment.

The free surface velocity profiles obtained during the experiments with the composite samples are shown by dots in Fig. 5. For convenience, the profiles are subsequently shifted along the velocity axis by 50 m/s one from the other. The six pairs of straight lines correspond to the acoustic approximation according to (2). In each pair the bottom line corresponds to the velocity $C_{\mathrm{L}}^{(\mathrm{c})}$ obtained from the ultrasonic measurements. In a manner similar to the one discussed for the epoxy samples, the upper lines were determined by assuming complete deterioration of the deviatoric component of the stress in the epoxy matrix. Thus, a simple estimate for the effective constrained Young modulus of the composite along the direction normal to the fibers plane can be obtained by regarding it as a laminated composite with alternating layers of the fibers and the matrix materials. For a laminate with glass and epoxy layers the constrained Young modulus is

$$\frac{1}{E'^{(\mathrm{c})}} = \frac{f^{(\mathrm{e})}}{E'^{(\mathrm{e})}} + \frac{f^{(\mathrm{g})}}{E'^{(\mathrm{g})}}, \tag{8}$$

where $f^{(\mathrm{e})} = 1 - f^{(\mathrm{g})}$ is the volume fraction of the epoxy phase. Moreover, since $E'^{(\mathrm{g})} \gg E'^{(\mathrm{e})}$ the constrained Young modulus of the composite may be approximated via the relation

$$\frac{1}{E'^{(\mathrm{c})}} \cong \frac{f^{(\mathrm{e})}}{E'^{(\mathrm{e})}}. \tag{9}$$

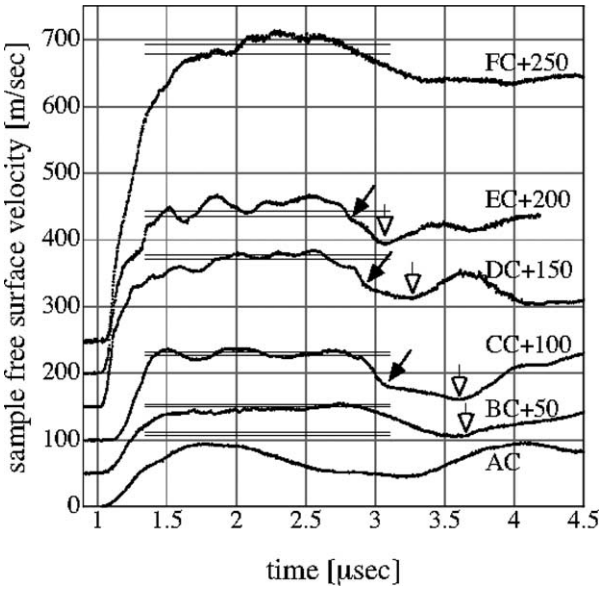

Fig. 5. Free surface velocity profiles measured for the composite samples.

Taking $f^{(e)} = 0.55$ in Eq. (9) we obtain $E'^{(c)} \cong 14.85$ GPa, indeed within the range of the ultrasonic measurements error ($E'^{(c)} = 15.2 \pm 0.4$ GPa). When the deviatoric component of the stress in the epoxy is relaxed, it behaves according to relation (5). The corresponding effective constrained Young's modulus of the composite can be estimated from Eq. (9) with $K^{(e)} = \rho_0 C_0$ instead of $E'^{(e)}$. Thus, $E'^{(c)}_\infty = K^{(e)}/f^{(e)} = 11.3$ GPa, and the corresponding sound velocity used for determining the values for the upper lines in each of the pairs shown in Fig. 5 is

$$C^{(c)}_\infty = \sqrt{E'^{(c)}_\infty/\rho^{(c)}} = 2480 \text{ m/s}. \tag{10}$$

We observe that the final state of the shocked composite is closer to the state represented by the upper set of lines.

The overall shapes of the recorded profiles are reminiscent of the ones predicted by Barker (1971), who demonstrated that laminated composites admit a viscous behavior even though the response of the constituents is strain rate independent. Here, the viscosity effects are further amplified since the behavior of one of the constituents is strain-rate dependent. The viscoelastic properties of the composite are determined by following steps similar to those followed for the epoxy. In this case, however, the overall relation between the strain and the stress (instead of between their deviators) is being analyzed. It is found that during the first 0.17 μs after the loading signal arrives at the free surface the behavior of the composite may be approximated by a Standard-linear model. We note that this time period is twice the fundamental period $T_0 = 0.085$ μs, closely the time it takes for the signal to travel across a 125 μm thick layer. Beyond this period there are effects of waves reflecting from the interface between the sub-layers. Thus, during the initial $2T_0$ time period the behavior of the composite is approximated via the relation

$$\dot{\varepsilon} = \frac{\dot{\sigma} - E'^{(c)}_\infty \dot{\varepsilon}}{E'^{(c)} - E'^{(c)}_\infty} + \frac{\sigma - E'^{(c)}_\infty \varepsilon}{\eta^{(c)}}, \tag{11}$$

where $\eta^{(c)}$ is the composite's effective viscosity. An estimate for $\eta^{(c)}$ can be extracted from the measurements of the stress, the strain and their rates in a manner similar to the one discussed for the epoxy samples. The

choice $\eta^{(c)} = 300$ Pa s provides a good approximation for the high velocity experiments DC, EC and FC. The effective relaxation time of the Maxwell branch in the model is $\tau^{(c)} = \eta^{(c)}/\left(E'^{(c)} - E'^{(c)}_{\infty}\right) \cong 77$ ns. We note that the relaxation time for the composite is almost identical to the one determined for the epoxy resin. This is in agreement with corresponding analytical findings of deBotton and Tevet-Deree (in press), who demonstrate that in the limit when the reinforcing fibers are markedly stiffer than the matrix, the effective relaxation time of the composite approaches that of the matrix material.

The steady waves existing in the composite sample may have or have not an initial shock-like component, depending on the amplitude of the impact. The shapes of profiles AC, BC and CC correspond to a free-of-shock response, while profile FC contains distinct shock-like component with an amplitude of about 150 m/s. A lower 120–130 m/s shock component may be revealed in the ramping part of the intermediate profiles DC and EC. We recall that the input stress pulse was rectangular in all the shots with the composite samples.

Oscillations of the free surface velocity, superimposed on the average velocity profiles of shots CC, DC, EC and FC can be identified. Lundergan and Drumheller (1971) observed oscillations of the particle velocity after planar impact loading of a composite containing 10 pairs of steel-epoxy plates produced by long impactor. Oved et al. (1978) observed strong oscillations of the signal measured by a manganine stress gauge embedded in a copper-PMMA laminated composite. The oscillations period found to be equal to twice the time taking for the signal to travel across a pair of layers. To extract the average contour of the stress pulse in a laminated composite, Barker (1971) introduced some randomization into the laminate geometry to avoid resonant and severe increase of the oscillations' amplitude.

In Fig. 5 it is apparent that the superimposed oscillations cannot be characterized by a single period. Thus for example, noting the profile for shot CC, the weakest one exhibiting oscillations, the first two maxima are separated by a 0.43 μs interval, while the time interval between the second and the third maxima is 0.72 μs. The most frequent maxima separation characteristic for shots DC and EC is 0.26 μs. In shot FC, although the velocity oscillations are strongly suppressed, characteristic oscillations with periods of 0.17 and 0.26 μs can be detected. All these time periods are integer products of the fundamental period $T_0 = 0.085$ μs. The stress signal propagating through this media acts as a driving force exciting these oscillations. Therefore, it is anticipated that with the increase of the impact intensity the consequences of more interactions between the propagating waves and the interfaces will be manifested at the free surface. As a result, an increase of the oscillations' frequency with the intensity of the impact is observed.

The mean peak-to-peak variations in the velocity profiles shown in Fig. 5 are 19, 32, 35 and 10 m/s (or less) for shots CC, DC, EC and FC, respectively. The decrease in the amplitude of the velocity oscillations during the strongest impact may be explained by the stronger decay of oscillations with higher frequencies. The imperfect periodicity of the composite preclude the resonance state observed in experiments with composites made out of perfectly alternating layers of two materials with different impedances. The dependence of the speed of sound in the epoxy phase on the compression level also contributes to the suppression of the resonance phenomenon.

The velocity oscillations introduce some distortions in the unloading parts of the velocity profiles and hence the analysis of the damaging processes in the fiber-reinforced composite is more complicated. The only sample which seemingly undergone the compression–tension cycle with no internal variations is the one from shot AC. The time interval between the first and the second velocity ramps corresponds to the time the wave traveled back and forth through the sample at a speed $C_L^{(c)} = 2880$ m/s. The second velocity ramp of the velocity profile for shot BC starts earlier than it should. This is due to the appearance of some, very modest yet feature which is marked by the light arrow. With the increase of the impact strength this feature is pronounced and turns into a usual spall signal during shot DC. Although the impact velocity in shot AC was slightly higher than the one in shot BC, the sample was not altered during the tension stage of the impact. This results from the twice longer compressive pulse in shot BC (a 6 mm thick impactor versus a 3 mm thick impactor in shot AC), which produced some incipient variation before the initiation of the

unloading stage. This compression generated variation is clearly noticeable in all the shots stronger than BC.

The unloading sections of profiles CC, DC and EC are characterized by two distinct regimes. The first, with a relatively fast velocity decrease, from the beginning of the unloading to the knee marked by a black arrow (see Fig. 5). The second, with a moderate slope, terminates with the appearance of the spall feature marked by the light arrow. The slope of the first regime depends on the impact strength in the same way as the slope along the loading section of the velocity profile. Subsequent occurrences are best explained with the aid of the time–distance diagram for shot DC shown in Fig. 6. Here, for convenience, we denote the various characteristics by their corresponding velocity in km/s. For the characteristics initiating at $t = 1.59$ μs, with the interaction of the unloading wave reflected from the impactor's back (free) surface with the impactor–sample interface, the letter "u" is added. The unloading wave velocities along these characteristics are determined by division of the sample's thickness by the time elapsed from the initiation of the characteristic to the time when the relevant signal was measured (these are marked with vertical dashed lines in Fig. 6a showing the free surface velocity profile).

The unloading starts with the arrival of the unloading characteristics denoted 2.88u (the left most dashed line in Fig. 6a). The second regime begins at $t = 2.95$ μs, with the arrival of the unloading characteristics denoted 2.27u corresponding to some variation in the material (the second to the left dashed line in Fig. 6a). In the absence of this material variation the surface should have continue its motion along the sharper slope of the previous profile segment. Subsequent unloading signals propagate with velocities lower than 2270 m/s through the just altered material located above the line marked D in Fig. 6b. The spall signal arrives with the characteristic marked 1.84u (the third dashed line in Fig. 6a). However, due to the variations in the material during the previous signals, the actual slope of this characteristic is unknown. Information concerning the nature of the fiber-reinforced composite spallation can be recovered from the section of the velocity profile corresponding to the reverberation of the stress pulse in the portion of the sample that was detached during the spall (the two right most dashed lines in Fig. 6a). The possible boundaries of the this

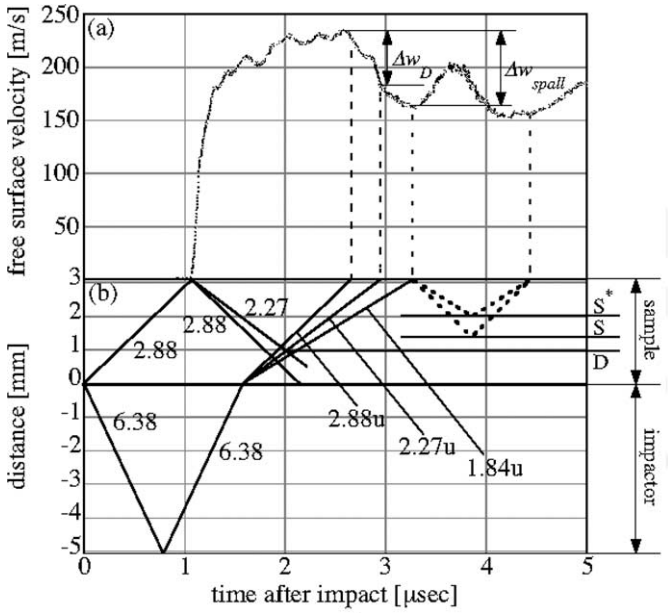

Fig. 6. A free surface velocity profile (a) and a time–distance diagram (b) for shot DC.

part are marked S and S* in Fig. 6b. These were determined by accounting for the highest (2880 m/s) and the lowest (1840 m/s) propagation velocities determined during the unloading section of the profile (the pair of characteristics represented by dashed lines at the right section of Fig. 6b). Since the maximum propagation velocity in the composite is 2880 m/s, the maximal distance between the sample's free surface and the spall plane is 1.7 mm (the line marked S in Fig. 6b). The thickness of the spall plate found after shot DC was 1.70 ± 0.01 mm. This suggests that the material variations prior to the spallation are reversible and may be interpreted in terms of a tensile stress relaxation.

The stress $\sigma_{\mathrm{D}}^{(\mathrm{c})}$ required for initiating this relaxation, as well as the spall stress $\sigma_{\mathrm{spall}}^{(\mathrm{c})}$, may be estimated from the corresponding velocity profiles by making use of approximation (7) previously used for estimating the spall stress of the epoxy (see estimates for Δw_{D} and $\Delta w_{\mathrm{spall}}$ during shot DC in Fig. 6a). The values of $\sigma_{\mathrm{D}}^{(\mathrm{c})}$ and $\sigma_{\mathrm{spall}}^{(\mathrm{c})}$ for each shot are listed in Table 3 along with the corresponding velocities. In a manner similar to the one followed for the epoxy, these stresses were calculated with both the measured longitudinal velocity $C_{\mathrm{L}}^{(\mathrm{c})}$ and the estimated velocity at the end of the relaxation process in the epoxy, $C_{\infty}^{(\mathrm{c})}$ of Eq. (10). We note that for the purpose of estimating the spall stress the usage of $C_{\infty}^{(\mathrm{c})}$ is probably more reasonable. This is because the spall stage initiates only after the process we denote as the tensile stress relaxation, will result in a relaxation of the deviatoric stress within the epoxy constituent.

On grounds of the stresses determined in Table 3 for shots CC, DC and EC we conclude that during shot BC a spall did not occur. The value $\Delta w_{\mathrm{D}} = 53$ m/s is close to the corresponding values obtained for shots CC and DC and is essentially smaller than the spall velocity pullback $\Delta w_{\mathrm{spall}} \cong 70$ m/s for the shots with evident spall. Moreover, interpretation of Δw_{D} for shot BC as a spall signal implies that, in passing from a 65 m/s impact (shot BC) to an 83 m/s impact (shot CC), $\sigma_{\mathrm{spall}}^{(\mathrm{c})}$ exhibits strong dependence on the rate of the tensile strain and varies by more than 30%. However, this conclusion contradicts the insensitivity of the spall strength on the rate of the tensile strain as exhibited in passing from shot CC to shot EC, where the difference in the impact velocities was markedly larger (70 m/s).

In shot EC the damage initiated early with $\Delta w_{\mathrm{D}} = 39$ m/s, less than the corresponding values for shots with lower impact velocities. Further, in shot FC there is no evidence for the existence of two distinct regimes in the unloading section of the velocity profile. This leads to the conclusion that the damage mechanism initiated during the compression stage. Since after shot DC the value of $\Delta w_{\mathrm{D}} = 54$ m/s is the same as the one for shots BC and CC, the maximum compressive pressure achieved in shot DC may be regarded as the composite's damage threshold in compression, $p_{\mathrm{th}}^{(\mathrm{c})} = 390$ MPa. However, although in shots EC and FC the unloading takes place in an already damaged substance, this damage is only partial and for both samples $\sigma_{\mathrm{spall}}^{(\mathrm{c})} = 150$ MPa, similar to the values measured for the undamaged samples. We further note that a comprehensive damage of the composite during the compression stage will result in the absence of the deceleration regime from the velocity profile (Zaretsky et al., 1997).

Reverberations of the signal in the spall-separated plate are absent from the velocity profile of shot FC and the remaining of the profile is horizontal. This situation is similar to the one previously discussed with regard to shot BE on the epoxy sample. Accordingly, the damage rate in the composite specimen $\dot{V}_{\mathrm{d}}^{(\mathrm{c})}$ is approximately four times the expansion rate $\dot{V}^{(\mathrm{c})}$, and the damaged zone is propagating from the spall

Table 3
Damage parameters of the fiber-reinforced composite

Shot	$w_{\max}$ [m/s]	w_{knee} [m/s]	Δw_{D} [m/s]	σ_{D} [MPa]	w_{spall} [m/s]	$\Delta w_{\mathrm{spall}}$ [m/s]	σ_{spall} [MPa]
AC	94	No knee	–	–	No spall	No spall	–
BC	101	48	53	140/120	No spall	No spall	–
CC	129	78	51	130/115	58	71	190/160
DC	239	185	54	140/120	167	72	190/160
EC	267	228	39	100/90	195	72	190/160
FC	459	No knee	–	–	389	70	180/160

toward the sample–impactor interface. This relation yields a damage rate $\dot{V}_{\mathrm{d}}^{(\mathrm{c})} = 45\ \mathrm{m}^3/\mathrm{kg\,s}$. After the shot, the corresponding portion of the composite sample was completely delaminated.

The spall strength of the composite (160 MPa) is lower than the spall strength measured for the epoxy samples (240 MPa), whereas the damage kinetics in the epoxy and the composite are approximately related via the relation $\dot{V}_{\mathrm{d}}^{(\mathrm{c})} \approx f^{(\mathrm{e})}\dot{V}_{\mathrm{d}}^{(\mathrm{e})}$. This suggests that the voids growth mechanism in the epoxy constituent is the dominant mechanism for voids growth in the composite and further highlights the role of the inter-constituent bonding with regards to the composite's spall strength. Thus, during the spallation of the homogeneous constituent the voids nucleation, their growth, and the subsequent coalescence into a fully developed spall, are essentially homogeneous processes. On the other hand, given that within the composite the interfaces provide plenty of voids nucleation sites, this process is obligatory heterogeneous. This easy voids nucleation process, which essentially results in a decrease of the composite's spall strength (Jacobi et al., 2000), implies that the composite's spall strength would always be lower than the spall strength of the resin.

4. Conclusions

Free surface velocity profiles of woven glass fibers reinforced epoxy composite and free-of-fibers epoxy samples were studied in a series of planar impact experiments at different impact velocities. The composite's behavior was investigated along the direction normal to the fibers plane, where it is anticipated that the properties of the resin will dominate the overall response. Low-velocity impacts were performed to examine the fundamental impact response of undamaged specimens. To examine the damage mechanism during the tensile and the compressive stages of the impact intermediate and high-velocity impacts were conducted.

During the loading stage the epoxy samples exhibited a viscoelastic behavior which is characterized by a dynamic viscosity $\eta^{(\mathrm{e})} = 110\ \mathrm{Pa\,s}$ and a relaxation time $\tau^{(\mathrm{e})} = 75\ \mathrm{ns}$. The release wave speed was substantially higher than the compression wave speed and decreased with a decrease of the pressure. The corresponding release isentrope for the shock-compressed epoxy was determined up to a pressure of 560 MPa. The estimated spall strength of the epoxy is in the range between 240 and 270 MPa, and the rate of the damage during the spall is $\dot{V}_{\mathrm{d}}^{(\mathrm{e})} \cong 66\ \mathrm{m}^3/\mathrm{kg\,s}$.

During the compression stage the response of the fiber-reinforced composite resembled that of a viscous solid with a dynamic viscosity $\eta^{(\mathrm{c})} = 300\ \mathrm{Pa\,s}$ and a corresponding stress relaxation time $\tau^{(\mathrm{c})} = 77\ \mathrm{ns}$. This finding is in agreement with the approach presented by Barker (1971) for modeling a layered composite as an effectively viscous solid with a single relaxation time. This is also in agreement with the form of the dependence exhibited by the initially rectangular stress pulses as they propagated through the composite. Thus, the free surface velocity profiles after weak impacts were free-of-shock whereas the profiles resulted from strong impacts contained a shock component.

Oscillations of the free surface velocity with periods which are integral products of the period taking for the signal to reverberates between two adjacent layers were measured. The imperfect periodicity of the composite's microstructure resulted in a relatively small oscillations, in contrast with the large oscillations at the resonance frequency which typically develop in composites with a regular microstructure. Since the level of the oscillations increase with that of the excitation, it is anticipated that stronger impacts will result in a more pronounced oscillations at the free surface. As a consequence, during stronger impacts the oscillations' frequency will increase too. Indeed, it was found that weak impacts resulted in the appearance of a long period oscillations and, as the wave front became steeper, the period of the oscillations became smaller. The latter, however, resulted in a strong decay of the amplitudes of the high-frequency oscillations.

A complex dynamic damaging process was revealed for the fiber-reinforced composite. At impact pressure lower than a threshold $p_{\mathrm{th}}^{(\mathrm{c})} = 390\ \mathrm{MPa}$ no indications of pressure activated damage were encountered. The undamaged specimens can withstand dynamic tensile stresses up to $\sigma_{\mathrm{D}}^{(\mathrm{c})} \cong 140\ \mathrm{MPa}$ with no

apparent damage, and a fully developed spall appears when the tensile stress exceeds a spall strength $\sigma_{\text{spall}}^{(c)} \cong 160$ MPa. In-between these stresses a relaxation process of the tensile stresses takes place and, as a consequence, the fracture occurs at a later time. When the compressive pressure exceeds the threshold $p_{\text{th}}^{(c)}$, the spall occurs in a partially damaged material. The rate of the macroscopic damage in the composite, $\dot{V}_{\text{d}}^{(c)} = 45\ \text{m}^3/\text{s}$, is dominated by that of the epoxy constituent, whereas the composite's spall strength is lower than the one measured for the epoxy. The reason being the difference in the void nucleation mechanism that results in a much higher initial nucleation rate in the composite.

Acknowledgements

This work was supported by the Israel Science Foundation founded by the Israel Academy of Sciences and Humanities (grant 317/99-2). The authors would like to thank Dr. R. Tsemach for providing the materials and technical support. The authors also wishes to thank one of the reviewers for identifying a mistake in an earlier version of the manuscript.

References

Agbossou, A., 1995. Effects of interphase and impact strain rates on tensile off-axis behavior of unidirectional glass fiber composite: experimental results. Eng. Fract. Mech. 52, 923–934.

Barker, L.M., 1971. A model for stress wave propagation in composite materials. J. Comp. Mater. 5, 140–162.

Barker, L.M., Hollenbach, R.E., 1970. Shock wave studies of PMMA, fused silica and sapphire. J. Appl. Phys. 41, 4208–4226.

Barker, L.M., Hollenbach, R.E., 1972. Laser interferometer for measuring high velocities of any reflecting surface. J. Appl. Phys. 43, 4669–4675.

Barre, S., Chotard, T., Benzeggagh, M.L., 1996. Comparative study of strain rate effects on mechanical properties of glass fiber reinforced thermoset matrix composites. Composites 27A, 1169–1181.

Dandekar, D.P., Boteler, J.M., Beaulieu, P.A., 1998. Elastic constants and delamination strength of a glass-fiber-reinforced polymer composite. Composite Sci. Technol. 58, 1397–1403.

deBotton, G., Tevet-Deree, L., in press. The response of a fiber reinforced composite with a viscous matrix phase. J. Comp. Mater.

El-Habak, 1991. Mechanical behavior of woven glass fiber-reinforced composites under impact compression load. Composites 22, 129–134.

Holmes, B.S., Tsou, F.K., 1972. Steady shock waves in composite materials. J. Appl. Phys. 43, 957–961.

Jacobi, S., Zaretsky, E., Shvarts, D., 2000. Experimental examination and numerical NAG model analysis of spall sensitivity to microstructure in copper. J. de Physique IV 9, 805–810.

Kolsky, H., 1963. Stress Waves in Solids. Dover Publications, New York.

Lifshitz, J.M., 1976. Impact strength of angle ply fiber reinforced materials. J. Comp. Mater. 10, 92–101.

Lundergan, C.D., Drumheller, D.S., 1971. Propagation of stress waves in laminated plate composite. J. Appl. Phys. 42, 669–675.

Munson, D.E., May, R.P., 1972. Dynamically determined high-pressure compressibilities of three epoxy resin systems. J. Appl. Phys. 43, 962–971.

Munson, B.E., Schuler, K.W., 1971. Steady wave analysis of wave propagation in laminates and mechanical mixtures. J. Comp. Mater. 5, 286–304.

Munson, D.E., Boade, R.R., Schuler, K.W., 1978. Stress wave propagation in Al_2O_3-poxy mixtures. J. Appl. Phys. 49, 4797–4807.

Oved, Y., Luttwak, G., Rosenberg, Z., 1978. Shock wave propagation in layered composites. J. Comp. Mater. 12, 84–96.

Postma, G.W., 1955. Wave propagation in stratified medium. Geophysics 20, 780–806.

Schuler, K.W., 1970. Propagation of steady shock waves in polymethyl methacrylate. J. Mech. Phys. Solids 18, 277–293.

Syam, B., Homma, H., Nakazato, K., 2000. Fracture behaviors of GFRP plates subjected to impulsive loading. In: Fracture and Strength of Solids, Key Engineering Materials. Trans Tech Publications, Zurich-Uetikon.

Tay, T.E., Ang, H.G., Shim, V.P.W., 1995. An empirical strain rate-dependent constitutive relationship for glass-fiber reinforced epoxy and pure epoxy. Compos. Struct. 33, 201–210.

Tokheim, R.E., Erlich, D.C., Kobayshi, T., 1989. Characterization of spall in Kevlar/epoxy composite. In: Schmidt, S.C., Johnson, J.N., Davison, L.W. (Eds.), Shock Compression of Condensed Matter, pp. 473–476.

Tsou, F.K., Chou, P.C., 1969. Analytical study of Hugoniot in unidirectional fiber reinforced composites. J. Comp. Mater. 3, 500–514.

Utkin, A.V., 1993. Effect of initial failure rate on the formation of a spalling pulse. Prikladnaya Mekanika I Tekhnicheskaya Fizika 4, 140–146 (Translated by Plenum Publishing Corporation 1994).

Zaretsky, E., Igra, O., Zhuk, A.Z., Lash, A.A., 1997. Deformation modes in fiberglass under weak impact. J. Reinforced Plastics Composites 16, 321–331.

Zhuk, A.Z., Kanel, G.I., Lash, A.A., 1994. Glass–epoxy composite behavior under shock loading. J. de Physique IV 4 (8), 403–407.